Journal of Power Sources 198 (2012) 149–157

Contents lists available at SciVerse ScienceDirect

Journal of Power Sources

journal homepage: www.elsevier.com/locate/jpowsour

Effects of Nb and W additions on high-temperature creep properties of ferritic stainless steels for solid oxide fuel cell interconnect

Yung-Tang Chiu, Chih-Kuang Lin*

Department of Mechanical Engineering, National Central University, Jhong-Li 32001, Taiwan

ARTICLE INFO

Article history:
Received 13 August 2011
Received in revised form
19 September 2011
Accepted 20 September 2011
Available online 28 September 2011

Keywords:
Planar solid oxide fuel cell
Interconnect
Ferritic stainless steel
Creep properties
Laves phase
Precipitate strengthening

ABSTRACT

Tensile and creep properties of a newly developed ferritic stainless steel (Crofer 22 H) with additions of Nb and W for planar solid oxide fuel cell (pSOFC) interconnect are investigated at 25–800 °C. These properties are compared with those of another ferritic stainless steel (Crofer 22 APU) without Nb or W. A significantly improved tensile and creep strength of Crofer 22 H over Crofer 22 APU for pSOFC interconnect is found and attributed to a precipitation strengthening effect of the Laves phase. According to the creep stress exponent, activation energy, and microstructural observations, the superiority of Crofer 22 H over Crofer 22 APU in creep resistance at 650–800 °C involves a power-law dislocation creep mechanism interacting with an in situ precipitation strengthening mechanism. The relation between creep rupture time and applied stress for Crofer 22 H is well described by a simple power law. Larson–Miller relationship is also applied and shows good results in correlating the creep rupture time with applied stress and temperature for the Crofer 22 H steel. A significant coarsening of the Laves phase is responsible for the reduced improvement of creep resistance in Crofer 22 H at the low-stress, long-term region of 800 °C.

1. Introduction

An intermediate operation temperature between 600 and 800 °C is favorable to reduce system cost and enhance long-term stability in development of planar solid oxide fuel cells (pSOFCs) [1]. Interconnect is a critical component in pSOFC as it plays a very important role in structural and electrical connection of unit cells. The requirements of a pSOFC interconnect include good electrical conductivity, low permeability of oxygen and hydrogen, suitable thermal conductivity, good chemical stability, adequate mechanical strength and creep resistance, and compatible coefficient of thermal expansion (CTE) with other components in pSOFC [2]. Iron-based alloys are favorable interconnect materials in pSOFC stacks at an operating temperature below 800 °C due to their high ductility, excellent workability, and comparatively low cost in comparison with the expensive ceramic interconnects [1,2]. Cr-rich ferritic stainless steels are potential candidates for the pSOFC interconnect among the iron-based alloys [2–5]. Creep resistance of ferritic stainless steels used as an interconnect of a small thickness is considered as one of the primary factors for durable operation of a pSOFC system [6].

Thermal stresses induced by CTE mismatch and thermal gradient in a pSOFC stack should not be overlooked for design of a reliable pSOFC system [7,8]. They could induce creep deformation in metallic interconnects at a long-term high-temperature environment. The probability of generating cracks in metallic interconnects is increased with creep deformation. Eventually, gas leakage due to such excessive deformation and/or cracking would result in degradation of cell performance. Therefore, a comprehensive analysis of creep behavior of the metallic interconnect is necessary for evaluating the structural durability of a pSOFC stack.

For the metallic interconnects developed for pSOFC, their characteristics such as electrical conductivity, corrosion resistance, oxidation resistance, thermal behavior, Cr evaporation, and long-term stability have been studied [3,9–13]. However, relatively limited work has been done on the high-temperature mechanical properties of the metallic interconnect for pSOFC [14,15]. High-temperature tensile and creep properties have been studied for a Cr-rich ferritic stainless steel, Crofer 22 APU, used as an interconnect in pSOFCs [14]. Creep rupture strength of ferritic stainless steels can be enhanced with combined additions of Nb, W, and Si [15]. Fine Nb(C, N) precipitates formed by adding a small amount of Nb can improve effectively the high-temperature mechanical properties of ferritic steels [16–18]. W is a contributive element to increase creep rupture strength of steels through precipitation and/or solid-solution strengthening effects [15,19,20]. A ferritic stainless steel, Crofer 22 H, has recently been developed as a pSOFC interconnect material by adding small amounts of Nb and W into the previously developed Crofer 22 APU steel. It has been reported that electrical conductivity and oxidation resistance of Crofer 22

* Corresponding author. Tel.: +886 3 426 7340; fax: +886 3 425 4501.
E-mail address: t330014@cc.ncu.edu.tw (C.-K. Lin).

0378-7753/$ – see front matter © 2011 Elsevier B.V. All rights reserved.
doi:10.1016/j.jpowsour.2011.09.056

Table 1
Comparison of chemical composition of Crofer 22 H and Crofer 22 APU stainless steels tested (wt%).

Alloy	Fe	C	Cr	Mn	Si	Ti	Cu	S	P	Al	La	Nb	W
Crofer 22 H	Bal.	0.007	22.93	0.43	0.21	0.07	0.02	<0.002	0.014	0.02	0.08	0.51	1.94
Crofer 22 APU	Bal.	0.003	22.71	0.44	0.02	0.07	0.01	<0.002	0.004	0.01	0.09	–	–

H with additions of Nb and W are better than those of Crofer 22 APU [15,21–23]. As compared to the electrical resistivity of Crofer 22 APU with a range from 105 to 115 μΩ cm, the electrical resistivity of Crofer 22 H at 600–800 °C is reduced by 2–5% [21,22]. Area specific contact resistance (ASR) of Crofer 22 H at 800 °C is comparable with that of Crofer 22 APU and has values of 20–50 mΩ cm^2 [15,23]. After discontinuous oxidation in simulated anode gas (Ar–4% H_2–20% H_2O) for 5000 h, the weight gain in a Crofer 22 H specimen is less than that in a Crofer 22 APU one by 31% [15,23]. As part of a series of studies on the high-temperature mechanical properties of metallic interconnects and glass sealants for pSOFC [14,24–26], the high-temperature mechanical properties of the recently developed Crofer 22 H alloy are investigated in the current study. In particular, the effects of additions of Nb and W on the high-temperature tensile and creep properties of the Cr-rich ferritic stainless steels for pSOFC interconnect are characterized through comparisons of the results of Crofer 22 H and Crofer 22 APU alloys.

2. Experimental procedures

2.1. Material and specimen

The material used in the present study is a commercially available Crofer 22 H ferritic stainless steel supplied by the vendor in the form of cold-rolled, annealed plates with a thickness of 2.5 mm. The chemical compositions, given in weight percent, of Crofer 22 H and Crofer 22 APU steels are listed in Table 1 for comparison. Note that 0.51 wt% of Nb and 1.94 wt% of W are added in the alloy, as compared with the previously studied Crofer 22 APU [14]. From these plates, pin-loaded specimens with a gauge section of 40 mm in length and 6 mm in width were manufactured to comply with ASTM Standard E8 [27] for high-temperature tensile and creep tests. There is no further heat treatment performed on the specimens after machining. Details of the specimen geometry are given elsewhere [14].

2.2. Tensile and creep test

Uniaxial tensile tests were performed in air under a stroke rate of 2 mm min^{-1}. Testing temperatures were set at 25, 600, 650, 700, 750, and 800 °C to simulate the operating temperature range of pSOFCs. Each tested specimen was heated to the specified temperature at a heating rate of 25 °C min^{-1}. The specimen was held at the specified temperature for 15 min before the load was applied. Strain was measured using a commercial high-temperature axial extensometer with a 12-mm gauge length. The final elongation was determined by putting back together the two broken pieces of specimen and measuring the distance change between two original gauge marks. The 0.2% offset yield strength S_y and ultimate tensile strength S_{UTS} were determined from the engineering stress–strain curves. Creep tests were conducted under constant load at 650, 700, 750, and 800 °C. Similar to the tensile test, each specimen was held at the specified temperature for 15 min before applying the load. The creep strain-time and stress-rupture time relationships for the given steel at various temperatures were then obtained. Details of the experimental setup and procedures for the tensile and creep tests can be found in Ref. [14].

2.3. Microstructural and fractographic analyses

After the tensile and creep tests, fracture surfaces of the specimens were examined with scanning electron microscopy (SEM). In addition, some of the tensile and creep specimens were cut perpendicularly to the loading axis, ground, and polished for metallographic preparation and observation. The microstructural change, creep damages, and morphology of precipitates were then characterized and analyzed with SEM and transmission electron microscopy (TEM). The relevant precipitates in the microstructure were identified by energy dispersive spectrometry (EDS).

3. Results and discussion

3.1. Effect of temperature on tensile strength

Fig. 1 shows the engineering stress–strain curves of Crofer 22 H at temperatures of 25–800 °C. Note only the strain less than 20% is presented in Fig. 2 due to an upper limit of 20% of the high-temperature extensometer. Tensile properties of the Crofer 22 H steel at different temperatures are listed in Table 2. As shown in Table 2, elongation and reduction of area are increased with temperature. After high-temperature tensile test, the significant reduction of cross-sectional area can be regarded as a high-temperature softening effect. The ultimate tensile strength, yield strength, and Young's modulus are decreased with increasing temperature, as shown in Table 2. A remarkable drop of yield strength was observed between 700 and 750 °C with a reduction of 31% in yield strength. As compared with the tensile properties of Crofer 22 APU [14], Crofer 22 H has a better tensile strength at 25–800 °C. Comparisons of the yield strength of Crofer 22 H and Crofer 22 APU steels at temperatures from 25 to 800 °C are shown in Fig. 2. High-temperature tensile strength of Nb or W-added ferritic stainless steel is improved not only by a solid-solution strengthening effect but also by a precipitation strengthening effect [16,28]. A large number of Laves phase precipitates were observed in Crofer 22 H specimens before a tensile test, while they were not found

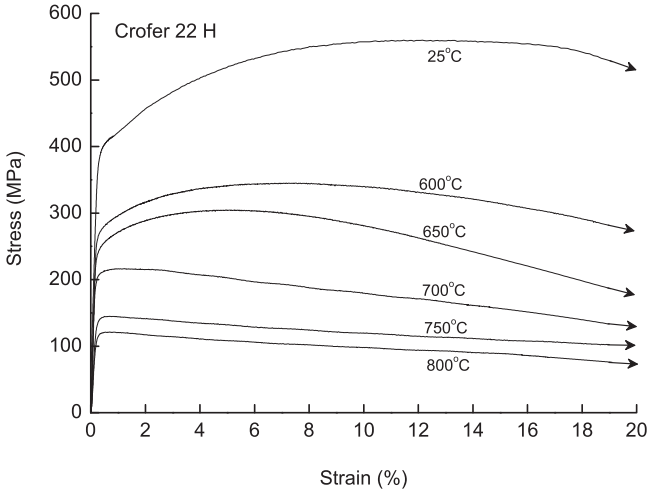

Fig. 1. Engineering stress–strain curves of Crofer 22 H at different temperatures in the range of strain less than 20%.

Table 2
Tensile properties of Crofer 22 H at various temperatures.

Temperature (°C)	Yield strength (MPa)	Ultimate tensile strength (MPa)	Young's modulus (GPa)	Elongation (in 12 mm) (%)	Reduction of area (%)
25	406	567	205	27	64
600	286	359	181	29	68
650	241	295	161	30	76
700	204	219	142	39	87
750	140	147	88	54	91
800	120	123	86	55	94

in Crofer 22 APU ones. Therefore, the superiority of Crofer 22 H over Crofer 22 APU in high-temperature tensile strength could be attributed to a precipitation strengthening effect of $(Fe,Cr)_2(Nb,W)$ Laves phase. Details of the microstructural analysis of Laves phase precipitates in the Crofer 22 H specimens are discussed in a later section.

As shown in Fig. 2, a significant reduction of 43% in yield strength occurs between 650 and 700 °C for Crofer 22 APU, while it takes place at a higher temperature range (700–750 °C) for the Crofer 22 H steel. It has been reported that addition of 0.5 wt% or more of Nb resulted in formation of $(Fe,Cr)_2Nb$ Laves phase in ferritic steels with a α-Fe(Cr) microstructure [29,30]. Ferritic steels with combined additions of W, Nb, and Si after exposure at 800 °C for 1000 h in air exhibited that a partial amount of W was dissolved in the Laves phase, leading to formation of $(Fe,Cr)_2(Nb,W,Si)$ Laves phase in the microstructure [15]. The yield strength in Nb-added ferritic stainless steels was significantly enhanced at around 700 °C in comparison with that in Ti-added steels due to a precipitation strengthening effect of the Laves phase [31]. Such an effect is also present in the current work, as 0.51 wt% of Nb and 1.94 wt% of W are added in Crofer 22 H in comparison with Crofer 22 APU. The yield strength of Crofer 22 H is about 1.4 times that of Crofer 22 APU at 25 and 600 °C. However, the yield strength ratio is increased with temperature, as the yield strength of Crofer 22 H is about 2.7 times that of Crofer 22 APU at 800 °C. In this regard, the tensile strength of Crofer 22 H with additions of Nb and W is better than that of Crofer 22 APU, particularly at higher temperatures.

3.2. Creep behavior

Creep strain curves for Crofer 22 H at different temperatures are shown in Fig. 3. As shown in Fig. 3, all the creep curves exhibit a relatively short period of primary creep as compared with the secondary stage. Apparently, strain hardening and recovery effects were rapidly balanced soon after the load was applied, leading to a constant, minimum creep strain rate. As also shown in Fig. 3, a longer rupture time is generated by a smaller applied stress at a given temperature. The following Arrhenius type of equation [32] is often used to correlate stress and temperature dependence of minimum creep rate:

$$\dot{\varepsilon}_{\min} = A\sigma^n \exp\left(\frac{-Q}{RT}\right) \quad (1)$$

where $\dot{\varepsilon}_{\min}$ is the minimum creep strain rate, σ is the applied stress, n is the stress exponent, Q is the apparent activation energy, R is the universal gas constant, T is the absolute temperature, and A is a constant. Creep behavior of the Crofer 22 APU steel was well described by such an equation [14]. Therefore, this equation is also applied to describe the stress dependence of minimum creep strain rate of the Crofer 22 H steel at various temperatures.

Fig. 4 shows the minimum strain rate as a function of applied stress for each creep curve of the Crofer 22 H steel presented in Fig. 3. Note creep curves of the Crofer 22 APU steel [14] are also plotted in Fig. 4 for comparison. In Fig. 4, the slope of each fitted straight line is the stress exponent (n). The relationship between minimum creep strain rate and applied stress follows a single power law at each temperature except for the Crofer 22 H steel at 800 °C. At 800 °C, a bilinear relation in log–log scale is observed for the Crofer 22 H steel. In the present study, n has a value of 17 at 650 °C, 18 at 700 °C, and 12 at 750 °C for Crofer 22 H, while at 800 °C, n has a value of 12 and 3 at the high- and low-stress region, respectively. However, n has a value of 5 at 650 °C and 700 °C and 6 at 750 °C and 800 °C for Crofer 22 APU, corresponding to a power-law dislocation creep mechanism [14]. Apparently, at each given temperature, Crofer 22 H has a greater n value than Crofer 22 APU except at the low-stress region of 800 °C. At a given temperature and applied stress, the minimum creep strain rate of Crofer 22 H is always lower than that of Crofer 22 APU. Such an improved creep resistance in the Crofer 22 H steel could be attributed to a precipitation strengthening effect of the Laves phase. A large number of Laves phase precipitates which were formed during steelmaking processes are observed in Crofer 22 H specimens, but not in Crofer 22 APU ones. The Laves phase can effectively retard dislocation motion, leading to a decrease in minimum creep strain rate. As shown in Fig. 4, the difference in minimum creep strain rate between Crofer 22 H and Crofer 22 APU steels at a given temperature is enlarged in the low-stress, long-term region except at 800 °C. At 650–750 °C, the precipitates are apparently more effective to hinder dislocation motion induced by a lower, applied stress than that by a higher stress level. It can be attributed to an in situ precipitation from the supersaturated solid solution in the matrix for a long-term creep test at 650–750 °C. In this regard, the minimum creep strain rate is more significantly reduced in the low-stress region for Crofer 22 H at 650–750 °C, leading to a much greater n value. In the low-stress region at a higher temperature such as 800 °C, an in situ precipitate coarsening effect took place in the Crofer 22 H steel during the long-term creep test. Such a precipitate coarsening effect could degrade the precipitation strengthening effect to a level lower than expected. This might explain why the Crofer 22 H steel at 800 °C exhibits two n values and a smaller n value of low-stress region

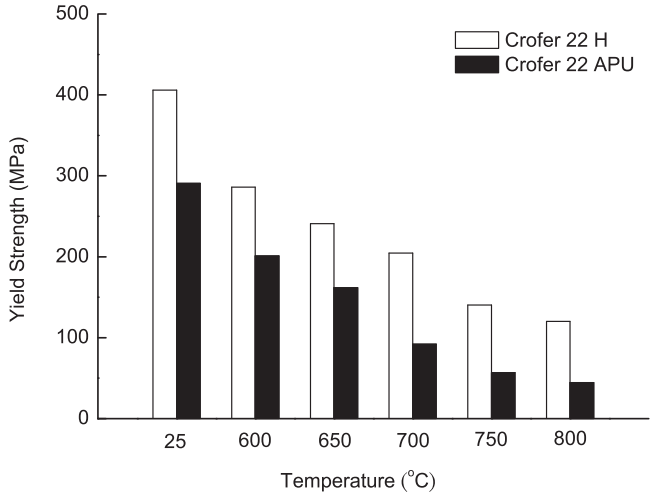

Fig. 2. Yield strength of Crofer 22 H and Crofer 22 APU steels at various temperatures.

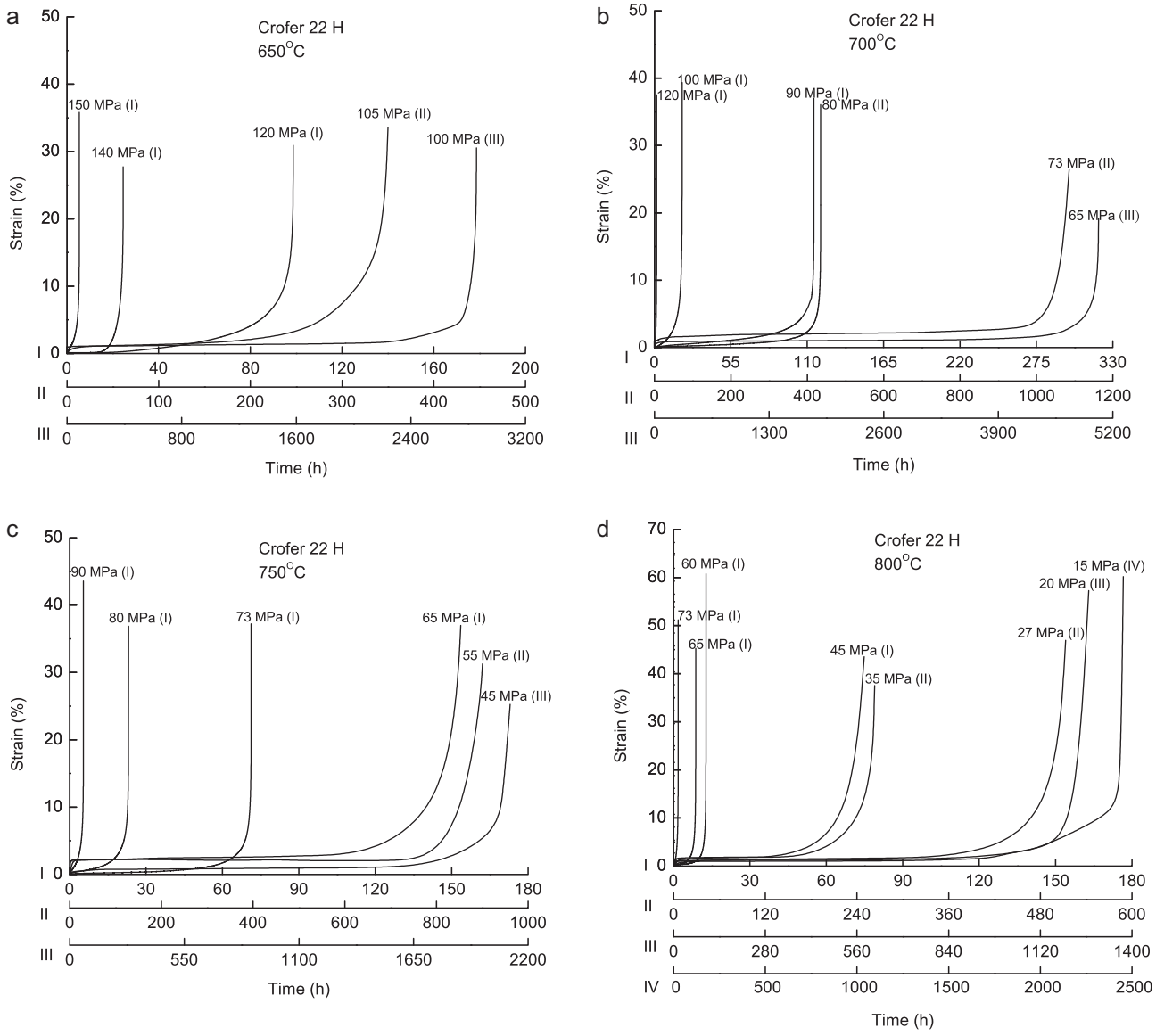

Fig. 3. Creep curves for Crofer 22 H at various temperatures: (a) 650 °C, (b) 700 °C, (c) 750 °C, and (d) 800 °C. (Note that three or four scales are used in the abscissa.)

in comparison with Crofer 22 APU. Details of the microstructural analysis of precipitate variation in the Crofer 22 H specimens are described in a later section.

As shown in Fig. 4, values of n for Crofer 22 H are reduced at 750–800 °C in comparison with those at 650–700 °C. The difference in minimum creep strain rate between Crofer 22 H and Crofer 22 APU steels in the high-stress region at 750–800 °C is apparently lager than that at 650–700 °C, due to a different extent of precipitation strengthening effect. A precipitation mechanism is expected to be more active at a higher temperature due to a greater driving force. It thus suggests that the in situ precipitation process take place and become effectively soon after the creep test started at a higher temperature like 750–800 °C. A value of 11 for creep stress exponent was observed in another Cr-rich ferritic steel with a precipitate strengthening effect when subjected to a creep loading [33]. Accordingly, the reduction of creep stress exponent from $n = 17$ or 18 at 650–700 °C to $n = 12$ at 750–800 °C except for the low-stress region of 800 °C in the current study is caused by an enhancement of precipitate strengthening effect. In addition, it has been reported that the variation of creep stress exponent (n) with temperature in a 9Cr heat resistant steel with an addition of W could be attributed to an effect of coarsening of precipitates [19]. A similar precipitate coarsening effect is responsible for the remarkable reduction of n value to 3 in Crofer 22 H in the low-stress region at 800 °C. It is expected that the precipitate coarsening mechanism is more active at 800 °C than at 650–750 °C. Consequently, the in situ precipitate coarsening mechanism in the low-stress, long-term creep test at 800 °C would lead to formation of a reduced number of precipitates with a larger size and spacing. Generally, stress required for a dislocation to by-pass a particle is inversely proportional to the inter-particle spacing [34]. Therefore, there is a reduction in the stress required for bending a dislocation if precipitates are distinctly spaced. The extent of improvement of creep resistance in Crofer 22 H over Crofer 22 APU is thus reduced at the low-stress region of 800 °C. A value of n in the range of 3–8 represents a dislocation type of creep mechanism [32]. The difference in the chemical composition between Crofer 22 H and Crofer 22 APU is the additions of Nb and W in the Crofer 22 H alloy. Therefore, the creep deformation mechanism of Crofer 22 H can be regarded as a power-law dislocation

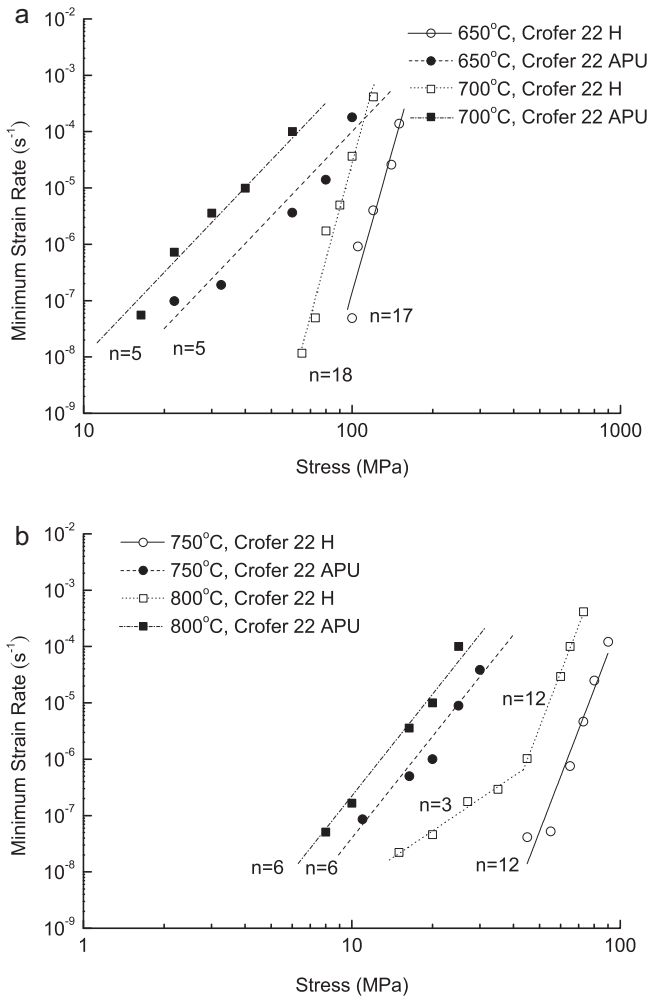

Fig. 4. Relationship between minimum creep strain rate and applied stress for Crofer 22 and Crofer 22 APU steels at various temperatures: (a) 650 °C and 700 °C; (b) 750 °C and 800 °C.

creep mechanism with interaction of a precipitation strengthening mechanism.

The apparent activation energy (Q) of Crofer 22 APU has been determined through Eq. (1) as 393 kJ mol^{-1} [14]. Eq. (1) is also applied to find the value of Q for Crofer 22 H in the present study. As shown in Fig. 5, the value of Q can be determined from the slope of the fitted straight line, by plotting logarithm of the product of minimum creep strain rate and reciprocal stress with a stress exponent of n versus logarithm of the reciprocal temperature for all the given stresses except low stresses at 800 °C. The low stresses of $n = 3$ at 800 °C were not involved in calculating the Q value due to a different creep mechanism. Accordingly, the apparent activation energy is estimated as 686 kJ mol^{-1} for the creep behavior of the Crofer 22 H stainless steel at 650–800 °C. Such a high value of Q is commonly observed in precipitation-strengthened alloys under creep deformation [33,35]. It means that additional thermal energy is required for a dislocation to overcome a large number of precipitates in Crofer 22 H as compared with Crofer 22 APU. In the current work, such a high value of Q for Crofer 22 H is associated with a power-law dislocation creep mechanism with interaction of a precipitation strengthening mechanism. Therefore, the apparent activation energy of Crofer 22 H is larger than that of Crofer 22 APU due to an effect of precipitation strengthening.

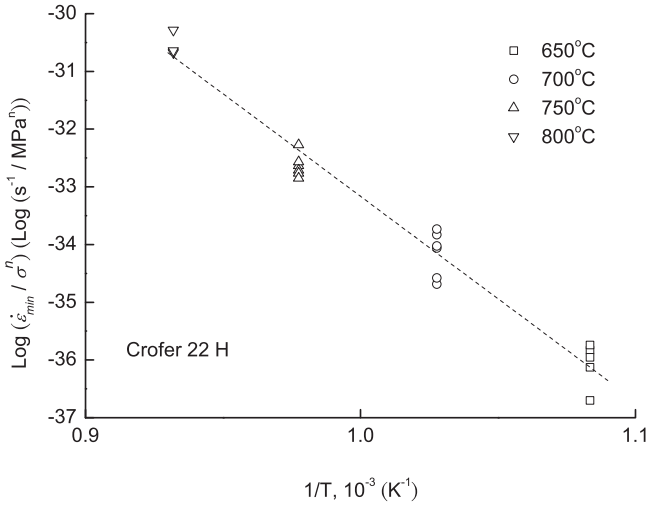

Fig. 5. Dependence of minimum creep strain rate and stress for Crofer 22 H steel at various temperatures except for low stresses at 800 °C.

3.3. Creep lifetime analysis

The relations between creep rupture time and applied stress for the Crofer 22 H and Crofer 22 APU steels at each given temperature are shown in Fig. 6. As shown in Fig. 6, the variation of creep rupture

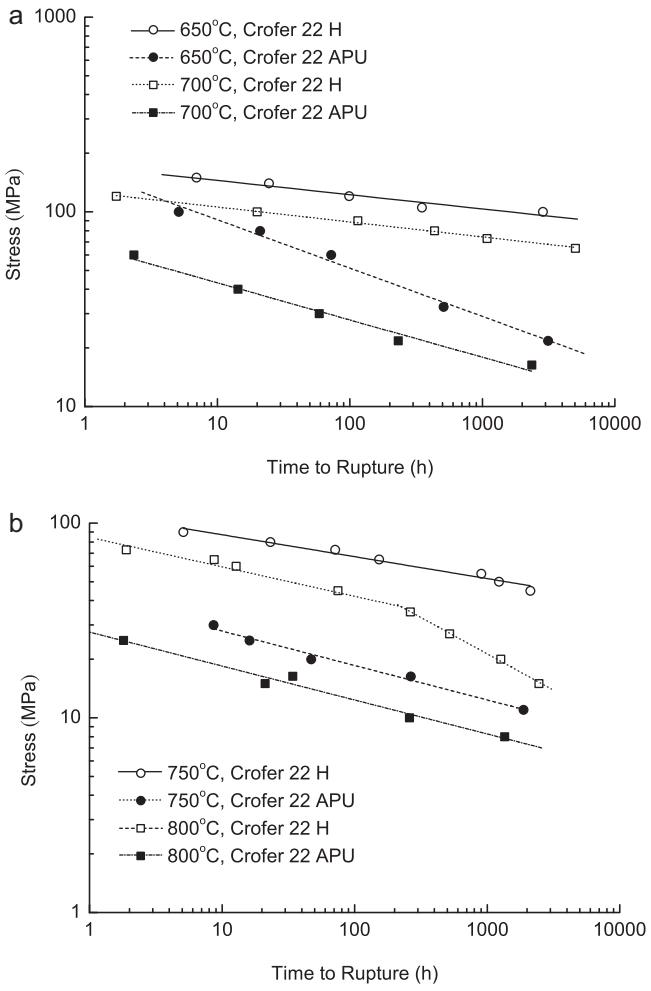

Fig. 6. Applied stress versus rupture time for Crofer 22 H and Crofer 22 APU steels at various temperatures: (a) 650 °C and 700 °C; (b) 750 °C and 800 °C.

time with applied stress for Crofer 22 H steel at each temperature follows a simple power law, except at 800 °C. The stress-rupture time relationship of Crofer 22 H in a log–log scale exhibits a bilinear curve at 800 °C, as shown in Fig. 6(b). It indicates that creep lifetime in the low-stress region at 800 °C is shorter than the expected lifetime following the trend of the high-stress region. Such a bilinear creep lifetime relationship at 800 °C could be attributed to the precipitate coarsening effect described above. The fitted equation and associated correlation coefficient for Crofer 22 H at each temperature in Fig. 6 are given as follows:

$$650\ ^\circ\text{C}: \quad \sigma t_r^{0.07} = 171, \quad r^2 = 0.94 \tag{2}$$

$$700\ ^\circ\text{C}: \quad \sigma t_r^{0.08} = 126, \quad r^2 = 1.0 \tag{3}$$

$$750\ ^\circ\text{C}: \quad \sigma t_r^{0.11} = 113, \quad r^2 = 0.98 \tag{4}$$

$$800\ ^\circ\text{C}\ (\text{high-stress region}, \quad \sigma \geq 45\,\text{MPa}): \quad \sigma t_r^{0.13} = 82.6, \quad r^2 = 0.96 \tag{5}$$

$$800\ ^\circ\text{C}\ (\text{low-stress region}, \quad \sigma < 45\,\text{MPa}): \quad \sigma t_r^{0.37} = 281, \quad r^2 = 1.0 \tag{6}$$

where σ is the applied stress in unit of MPa, t_r is the time to rupture in unit of h, and r is the correlation coefficient for each fitted curve. Variation of creep rupture time with applied stress for Crofer 22 H at 650–800 °C can be well described by these simple-power-law relations, as the correlation coefficient for each fitted curve shows a very large value from 0.94 to 1.0. Therefore, the creep rupture time of Crofer 22 H can be estimated through these power-law relations once the applied stress is known.

As shown in Fig. 6, creep rupture time of Crofer 22 H is significantly longer than that of Crofer 22 APU at a given stress and temperature. In addition, the difference in creep rupture time between the two steels increases with a decrease in applied stress at each given temperature except at the low-stress region of 800 °C. This can be explained by the aforementioned in situ precipitation mechanism taking place during the creep test of Crofer 22 H steels. As the creep testing time became longer and longer, more and more precipitates were formed in the Crofer 22 H specimens to enhance their creep resistance in comparison with Crofer 22 APU ones. At 800 °C, the difference of creep lifetime between the given two steels at the low-stress region is smaller than expected, due to a lessening precipitation strengthening effect counteracted by a precipitate coarsening mechanism. In general, the improved creep resistance of the Crofer 22 H steel with additions of Nb and W can be attributed to a precipitation strengthening effect.

A well-known Larson–Miller relationship [32] is also applied in the present study to correlate the creep lifetime with applied stress and temperature. Such a Larson–Miller relation has been shown to well describe the creep rupture time at 650–800 °C for the Crofer 22 APU steel [14]. The relationship is expressed as below:

$$P_{LM} = T(\log\ t_r + C) \tag{7}$$

where P_{LM} is the Larson–Miller parameter with a function of applied stress, T is temperature in Kelvin scale, and t_r is in unit of h. C is a constant and its value can be determined by extrapolating an intercept of $\log t_r = -C$ at $1/T = 0$ on a plot of $\log t_r$ versus $1/T$. In this way, the values of C for Crofer 22 H at the given temperatures were determined as 22.7–38.5. Values of C are often close to 20 for various steels and engineering metals [36]. In the present study, an average value of 27.9 was adopted for the constant C in Eq. (7). Values of P_{LM} calculated by Eq. (7) can then be plotted against stress, as shown in Fig. 7. The fitted master curve of the Larson–Miller parameter for the Crofer 22 H steel is given as follows:

$$\sigma = -3.78 \times 10^{-10} P_{LM}^3 + 3.44 \times 10^{-5} P_{LM}^2 - 1.06 P_{LM} + 1.10 \times 10^4, \quad r^2 = 0.99 \tag{8}$$

where σ is in unit of MPa. The Larson–Miller parameter and applied stress are well correlated by such a polynomial relationship for Crofer 22 H at different temperatures due to the high value of correlation coefficient. In this regard, the creep rupture time of pSOFC interconnects made of Crofer 22 H at variously combined stress and temperature can be predicted by Eqs. (7) and (8).

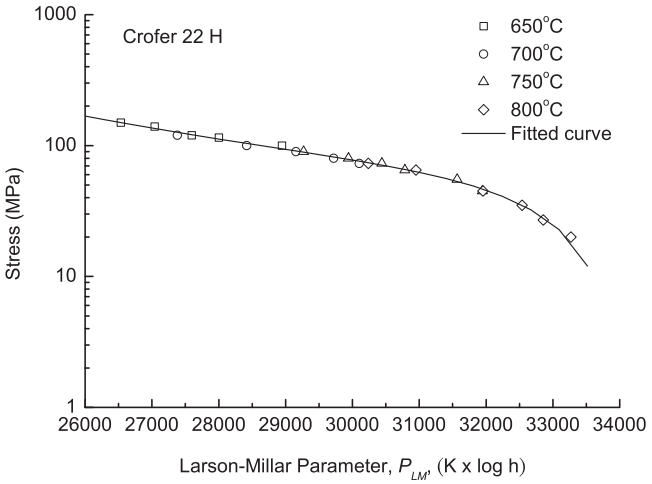

Fig. 7. Master curve of Larson–Miller parameter for Crofer 22 H steel.

3.4. Microstructural and fractography analysis

Representative SEM micrographs of the fracture surface of Crofer 22 H specimens after creep test are shown in Fig. 8. The remarkable reduction of fractured cross-sectional area shown in

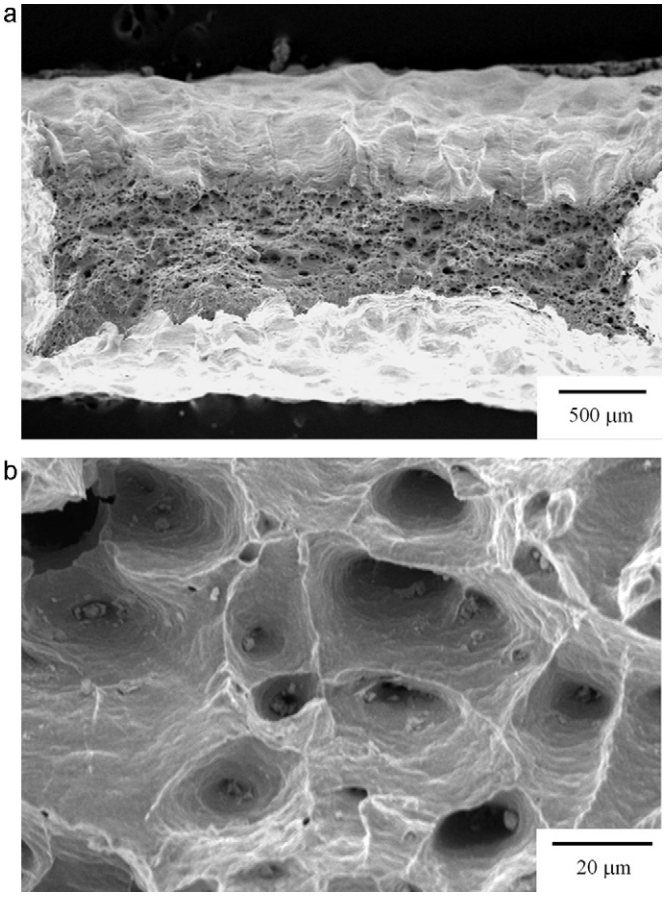

Fig. 8. Fractographs of a Crofer 22 H specimen after creep test at 700 °C: (a) low magnification; (b) high magnification.

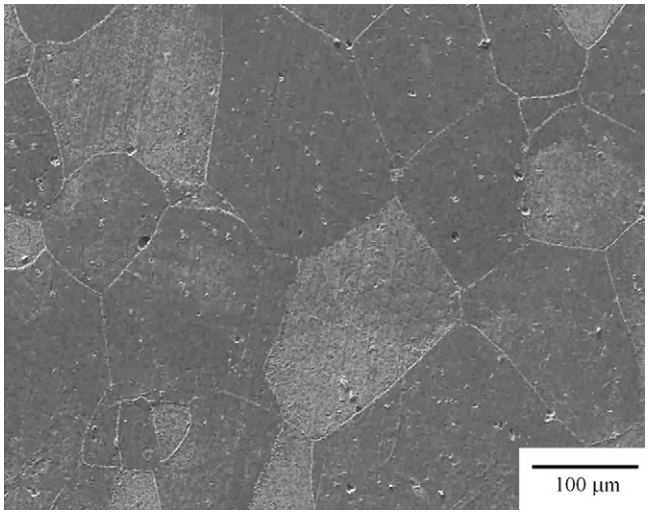

Fig. 9. SEM micrograph of microstructure in the Crofer 22 H specimen before creep test.

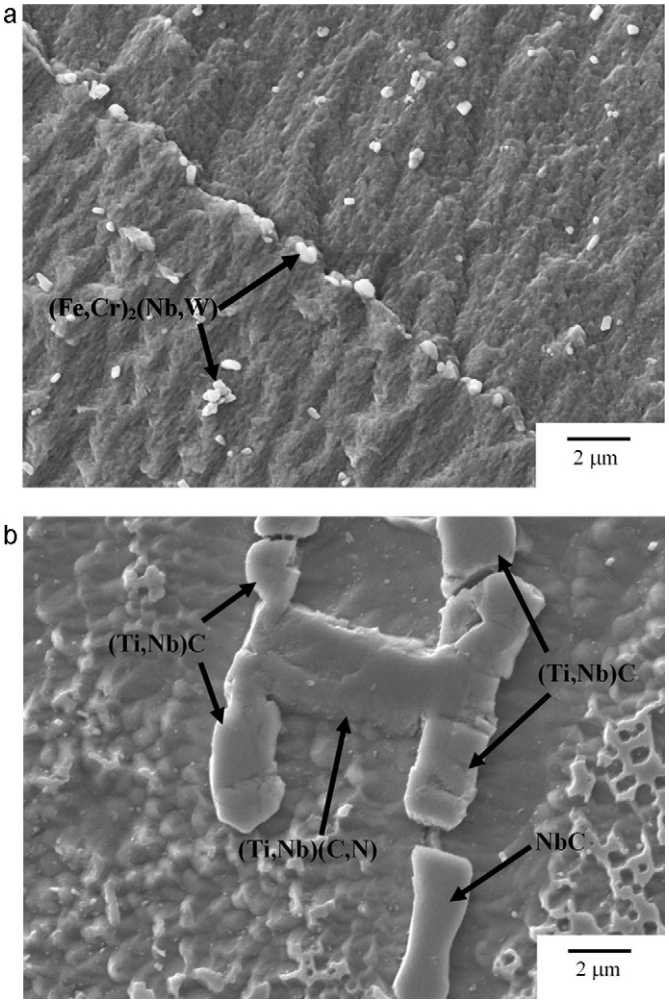

Fig. 10. SEM micrographs of precipitates of (a) $(Fe,Cr)_2(Nb,W)$ and (b) NbC, (Ti,Nb)C, and (Ti,Nb)(C,N) in a Crofer 22 H specimen before creep test.

Fig. 8(a) results from a necking behavior in the tertiary creep region. Such a reduction of cross-sectional area during creep test can be attributed to a high-temperature softening effect. In addition, the tendency of formation of microvoids is increased through a triaxial stress state induced by the necking behavior. Such microvoids are mostly formed around precipitates by interface decohesion between particles and the matrix. Finally, enhanced growth and coalescence of microvoids during the tertiary creep stage resulted in a ductile fracture of specimens. A ductile failure pattern is evidenced by the dimpled features shown in Fig. 8(b). As also shown in Fig. 8(b), the existence of particles inside microvoids is an evidence to confirm that precipitates are nucleation sites of microvoids. An SEM micrograph of a surface-sectional view of the Crofer 22 H specimens before tensile or creep test is shown in Fig. 9. The micrograph in Fig. 9 shows ferritic grain boundaries and the average grain size is about 155 μm. Voids and some precipitates, detected as Laves phase particles ($(Fe,Cr)_2(Nb,W)$), carbides (NbC and (Ti,Nb)C), and carbonitrides ((Ti,Nb)(C,N)), are also observed in the microstructure. Note that the Laves phase precipitates were identified by TEM-EDS analysis because of their small size. The voids were presumably left by the debonded precipitates during metallography specimen preparation. Typical morphologies of the Laves phase particles, carbides, and carbonitrides in the Crofer 22 H steel before creep test are shown in Fig. 10. In addition to the carbides and carbonitrides shown in Fig. 10(b), a large number of Laves phase precipitates with very small sizes (Fig. 10(a)) were formed in Crofer 22 H. As shown in Fig. 10(a), Laves phase precipitates are distributed within grains and mostly at grain boundaries before creep test. Such Laves phase precipitates observed in the Crofer 22 H steel were not found in the Crofer 22 APU steel. In contrast to the fine Laves phase particles in Crofer 22 H, scattered precipitates of TiN with a larger size were observed in the crept Crofer 22 APU specimens [14]. Therefore, Crofer 22 H has better tensile and creep properties than does Crofer 22 APU, mainly due to existence of such Laves phase precipitates. Improved tensile strength and creep resistance of a similar 22% Cr ferritic steel were also found to be related to a precipitation strengthening effect of fine Laves phase particles of $(Fe,Cr)_2(Nb,W)$ in a recent study [37].

Representative TEM micrographs of the Crofer 22 H microstructure before and after creep test at different conditions are shown in Fig. 11. In Fig. 11, the rod-shaped particles are identified as the Laves phase and the wires are dislocation lines. Laves phase particles can be nucleated and precipitated within grains and mostly at grain boundaries, by means of thermal energy during creep test. As grain boundaries are surface defects in a microstructure, nucleation of precipitates most easily occurs at grain boundaries, thereby minimizing surface energy [38]. Therefore, the number of Laves phase precipitates in the crept Crofer 22 H specimens increases through an in situ precipitation mechanism during creep test as compared with that before creep test, except for the low-stress region at 800 °C, as shown in Fig. 11. Subgrain boundaries found in Fig. 11(b) were formed by movement of dislocation induced by the applied creep loading. An increase in the number of Laves phase precipitates with a smaller spacing can effectively hinder such dislocation motion, as shown in Fig. 11(b) and (c). In comparison with the distributive, fine Laves phase particles observed at 700 °C in Fig. 11(b), a coarse Laves phase particle is found in Fig. 11(d) for a long-term creep test specimen at 800 °C. It is believed that large Laves phase particles would grow during a long-term high-temperature creep test at the expense of the smaller ones due to an in situ precipitate coarsening mechanism. Therefore, the number of Laves phase particles present in Fig. 11(d) is significantly reduced, but the size is much larger. Again, the significantly improved creep resistance in Crofer 22 H over Crofer 22 APU is primarily attributed to existence of such Laves phase precipitates. The extent of improvement depends on the number and size of Laves phase particles.

Table 3 lists the average particle size of the Laves phase within grains and at grain boundaries in Crofer 22 H steels before and after creep test. As shown in Table 3, the average particle size of the Laves phase after creep test is larger than that before creep

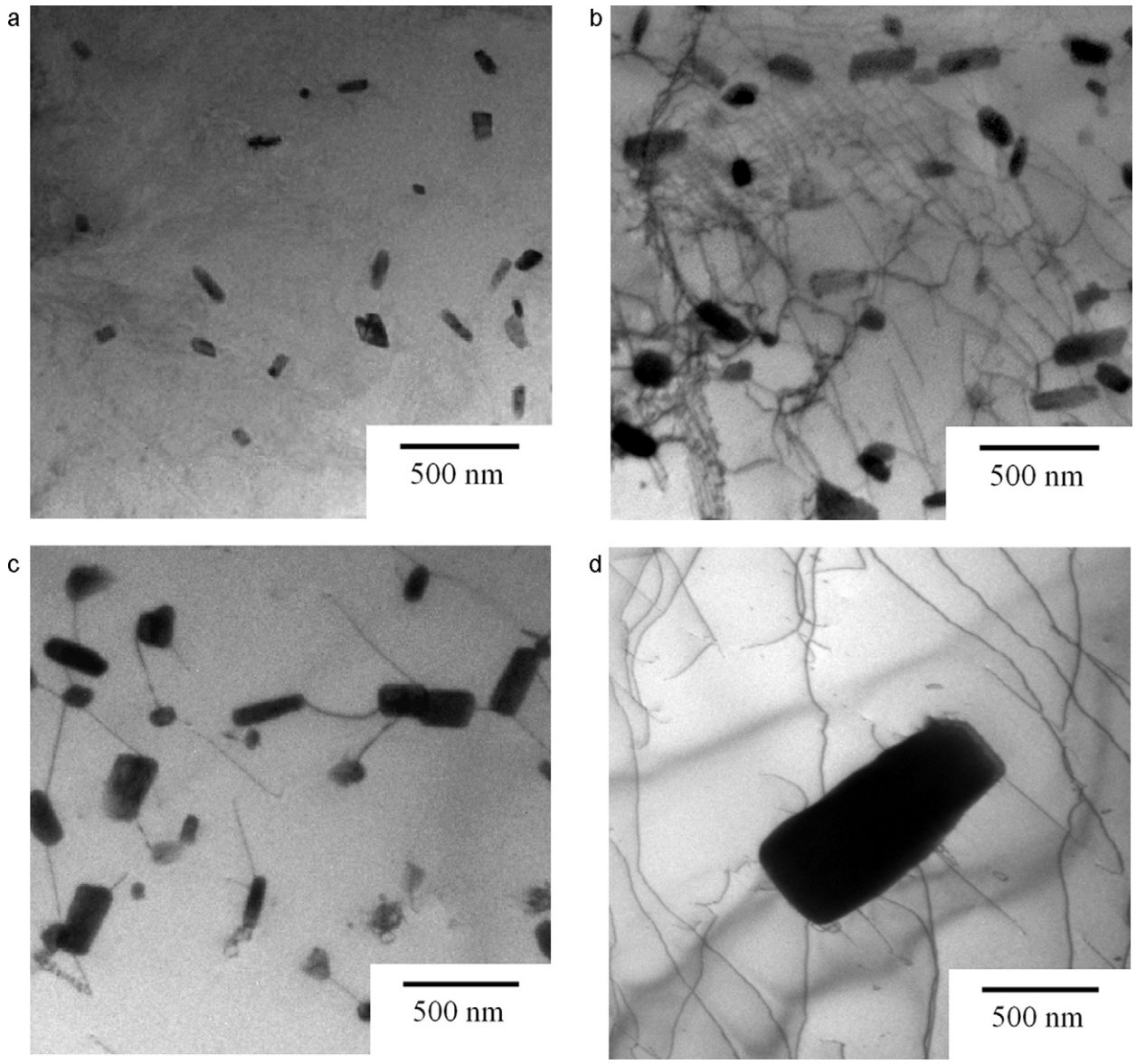

Fig. 11. TEM micrographs of the Crofer 22 H microstructure before and after creep test at various conditions: (a) before creep test; (b) 65 MPa, 5040 h, 700 °C; (c) 45 MPa, 2113 h, 800 °C; (d) 15 MPa, 2453 h, 800 °C.

test, and the difference is increased with creep testing temperature and time. In addition, growth of the Laves phase at grain boundaries is faster than that within grains during creep deformation. Generally, grain boundary diffusion is faster than lattice diffusion, promoting preferential diffusion of Nb and W atoms in the vicinity of grain boundaries into the Laves phase precipitates at grain boundaries. As a result, the extent of increase of Laves phase particle size after creep test is significantly greater at grain boundaries than that within grains. As shown in Table 3, given a comparable long-term creep rupture time (2xxx h), the Laves phase precipitates at 650 °C are smaller than those at 750 and 800 °C. Therefore, the effect of temperature on the growth of Laves phase particles during creep test is significant at the given testing temperature range. Additionally, the Laves phase precipitates in a creep test with the longest lifetime (5040 h) at 700 °C are larger than those at 750 °C (2113 h), indicating a partial effect of creep testing time on growth

Table 3
Average particle sizes of the Laves phase in Crofer 22 H steels before and after creep test at various conditions.

Testing temperature (°C)	Applied stress (MPa)	Time to rupture (h)	Average particle size (nm)	
			Within grains	At grain boundaries
Before creep test	–	–	150	191
650	100	2858	151	571
700	65	5040	163	646
750	45	2113	152	606
800	45	74.9	179	396
800	15	2453	1388	2071

of the Laves phase. Although the testing time of a short-term creep test (74.9 h) at 800 °C in Table 3 is the shortest among the conditions compared, its average particle size of the Laves phase within grains is larger than those at 650–750 °C. As creep testing temperature of 800 °C is greater than half of the absolute melting temperature of Crofer 22 H, lattice diffusion at such a high temperature becomes more active. It thus indicates that the testing temperature is the primary factor in influencing the growth of Laves phase particles during creep test.

The Laves phase with a size of about 100–200 nm has a beneficial effect on creep strength for ferritic steels [39]. However, when Laves phase precipitates coarsen to a size above 1000 nm, creep strength is reduced [39]. In the present work, Laves phase precipitates have a size of less than 1000 nm after creep test at various temperatures except the low-stress region of 800 °C. The ability of the scattered, coarse Laves phase precipitates to retard dislocation motion is reduced as compared with the distributive, fine ones. Therefore, the precipitation strengthening effect of the Laves phase is decreased in the long-term creep region at 800 °C in comparison with that at 650–750 °C and at the short-term region of 800 °C. Meanwhile, growth of the Laves phase precipitates lessens the content of W in the matrix and leads to a decrease in creep strength by counteracting the solid-solution strengthening effect [40]. As a result, significant coarsening of the Laves phase precipitates is responsible for a less enhancement of creep strength in the long-term region at 800 °C for the Crofer 22 H steel.

4. Conclusions

1. High-temperature tensile strength of the Crofer 22 H steel with additions of Nb and W is superior to that of Crofer 22 APU. It could be attributed to a precipitation strengthening effect of $(Fe,Cr)_2(Nb,W)$ Laves phase. The yield strength ratio of Crofer 22 H to Crofer 22 APU is increased with testing temperature.
2. Additions of Nb and W in the Crofer 22 H steel enhance the creep resistance by reducing the creep strain rate. The difference in minimum creep strain rate between Crofer 22 H and Crofer 22 APU steels at each given temperature is increased in the low-stress, long-term region except at 800 °C. The improved creep resistance of Crofer 22 H over Crofer 22 APU at 650–800 °C is attributed to a power-law dislocation creep mechanism with interaction of an in situ precipitation strengthening mechanism. The extent of improvement is reduced at the long-term region of 800 °C due to a precipitate coarsening effect.
3. The relation between creep rupture time and applied stress in Crofer 22 H is well fitted by a single power law at 650–750 °C, while it exhibits a bilinear curve in a log–log scale at 800 °C. Creep rupture time of the Crofer 22 H steel is also well described by the Larson–Miller relation for various combinations of applied stress and temperature. Given a stress and temperature, the creep rupture time of Crofer 22 H is much longer than that of Crofer 22 APU by more than two orders of magnitude.
4. Crofer 22 H shows better tensile and creep properties than Crofer 22 APU, mainly due to existence of $(Fe,Cr)_2(Nb,W)$ Laves phase precipitates. The number of Laves phase precipitates in the crept Crofer 22 H specimens increases through an in situ precipitation mechanism during creep test except at the low-stress, long-term region of 800 °C. In the latter, the number of Laves phase precipitates is reduced but the size is significantly increased due to a precipitate coarsening effect.

Acknowledgement

This work was supported by the National Science Council (Taiwan) under Contract No. NSC 99-2221-E-008-012-MY3.

References

[1] A. Weber, E. Ivers-Tiffée, J. Power Sources 127 (2004) 273–283.
[2] W.Z. Zhu, S.C. Deevi, Mater. Sci. Eng. A 348 (2003) 227–243.
[3] I. Antepara, I. Villarreal, L.M. Rodriguez-Martinez, N. Lecanda, U. Castro, A. Laresgoiti, J. Power Sources 151 (2005) 103–107.
[4] J.W. Fergus, Mater. Sci. Eng. A 397 (2005) 271–283.
[5] K. Huang, P. Hou, J. Goodenough, Solid State Ionics 129 (2000) 237–250.
[6] P. Lamp, J. Tachtler, O. Finkenwirth, S. Mukerjee, S. Shaffer, Fuel Cells 3 (2003) 146–152.
[7] C.-K. Lin, T.-T. Chen, Y.-P. Chyou, L.-K. Chiang, J. Power Sources 164 (2007) 238–251.
[8] C.-K. Lin, L.-H. Huang, L.-K. Chiang, Y.-P. Chyou, J. Power Sources 192 (2009) 515–524.
[9] H. Kurokawa, K. Kawamura, T. Maruyama, Solid State Ionics 168 (2004) 13–21.
[10] Z. Yang, G.-G. Xia, M.S. Walker1, C.-M. Wang, J.W. Stevenson, P. Singh, Int. J. Hydrogen Energy 32 (2007) 3770–3777.
[11] S.J. Geng, J.H. Zhu, Z.G. Lu, Solid State Ionics 177 (2006) 559–568.
[12] P.E. Gannon, C.T. Tripp, A.K. Knospe, C.V. Ramana, M. Deibert, R.J. Smith, V.I. Gorokhovsky, V. Shutthanandan, D. Gelles, Surf. Coat. Technol. 188–189 (2004) 55–61.
[13] S. Fontana, R. Amendola, S. Chevalier, P. Piccardo, G. Caboche, M. Viviani, R. Molins, M. Sennour, J. Power Sources 171 (2007) 652–662.
[14] Y.-T. Chiu, C.-K. Lin, J.-C. Wu, J. Power Sources 196 (2011) 2005–2012.
[15] J. Froitzheim, G.H. Meier, L. Niewolak, P.J. Ennis, H. Hattendorf, L. Singheiser, W.J. Quadakkers, J. Power Sources 178 (2008) 163–173.
[16] N. Fujita, K. Ohmura, M. Kikuchi, T. Suzuki, S. Funaki, I. Hiroshige, Scr. Mater. 35 (1996) 705–710.
[17] T. Onizawa, T. Wakai, M. Ando, K. Aoto, Nucl. Eng. Des. 238 (2008) 408–416.
[18] G.-M. Sim, J.-C. Ahn, S.-C. Hong, K.-J. Lee, K.-S. Lee, Mater. Sci. Eng. A 396 (2005) 159–165.
[19] F. Abe, Mater. Sci. Eng. A 319–321 (2001) 770–773.
[20] J. Hald, Steel Res. 67 (1996) 369–374.
[21] Material Data Sheet of Crofer 22 APU. http://www.thyssenkrupp-vdm.Com/en/downloads/data-sheets/?no_cache=1 (accessed 18.09.11).
[22] Material Data Sheet of Crofer 22 H. http://www.thyssenkrupp-vdm.com/en/downloads/data-sheets/?no_cache=1 (accessed 18.09.11).
[23] L. Paul, H. Hattendorf, L. Niewolak, B. Kuhn, O. Ibas, W.J. Quadakkers, Proceedings of Fuel Cell Seminar 2010, San Antonio, TX, USA, October 2010.
[24] H.-T. Chang, C.-K. Lin, C.-K. Liu, J. Power Sources 189 (2009) 1093–1099.
[25] H.-T. Chang, C.-K. Lin, C.-K. Liu, J. Power Sources 195 (2010) 3159–3165.
[26] H.-T. Chang, C.-K. Lin, C.-K. Liu, S.-H. Wu, J. Power Sources 196 (2011) 3583–3591.
[27] ASTM Standard E8/E8M-09, Standard Test Method for Tension Testing of Metallic Materials, ASTM International, West Conshohohocken, PA, USA, 2009, pp. 1–27.
[28] S.G. Hong, W.B. Lee, C.G. Park, J. Nucl. Mater. 288 (2001) 202–207.
[29] N. Fujita, K. Ohmura, A. Yamamoto, Mater. Sci. Eng. A 351 (2003) 272–281.
[30] K. Yamamoto, Y. Kimura, F.-G. Wei, Y. Mishima, Mater. Sci. Eng. A 329–331 (2002) 249–254.
[31] A. Miyazaki, K. Takao, O. Furukimi, Iron Steel Inst. Jpn. 42 (2002) 916–920.
[32] N.E. Dowling, Mechanical Behavior of Materials, 3rd ed., Pearson Education, Inc., NJ, USA, 2007, pp. 779–797.
[33] S.C. Tjong, Z.Y. Ma, Mater. Lett. 56 (2002) 59–64.
[34] E. Arzt, D.S. Wilkinson, Acta Metall. 34 (1986) 1893–1898.
[35] G. Schoeck, Phys. Stat. Sol. 8 (1965) 499–507.
[36] M.E. Kassner, T.A. Hayes, Int. J. Plasticity 19 (2003) 1715–1748.
[37] B. Kuhna, C.A. Jimeneza, L. Niewolaka, T. Hüttela, T. Becka, H. Hattendorfb, L. Singheisera, W.J. Quadakkersa, Mater. Sci. Eng. A 528 (2011) 5888–5899.
[38] D.R. Askeland, P.P. Fulay, Essentials of Materials Science and Engineering, 2nd ed., Cengage Learning, Inc., FL, USA, 2010, pp. 358–364.
[39] J. Hald, Z. Kubon, J. Hald, Z. Kubon, in: A. Strang, D.J. Gooch (Eds.), Microstructural Development and Stability in High Chromium Ferritic Power Plant Steels, Institute of Materials, Cambridge, 1997, pp. 159–178.
[40] V. Sklenicka, K. Kucharova, M. Svoboda, L. Kloc, J. Bursik, A. Kroupa, Mater. Charact. 51 (2003) 35–48.